Organic Electronics 13 (2012) 166–172

Contents lists available at SciVerse ScienceDirect

Organic Electronics

journal homepage: www.elsevier.com/locate/orgel

Solution-processable star-shaped photovoltaic organic molecules based on triphenylamine and benzothiadiazole with longer pi-bridge

Jing Zhang, Jintao Yu, Chang He *, Dan Deng, Zhi-Guo Zhang, Miaojie Zhang, Zhibo Li, Yongfang Li *

Beijing National Laboratory for Molecular Sciences, Institute of Chemistry, Chinese Academy of Sciences, Beijing 100190, China

ARTICLE INFO

Article history:
Received 24 August 2011
Received in revised form 27 October 2011
Accepted 30 October 2011
Available online 15 November 2011

Keywords:
Organic solar cells
Star-shaped photovoltaic organic molecules
Solution-processability

ABSTRACT

Two solution-processable star-shaped D–π–A organic molecules with triphenylamine (TPA) as donor unit, benzothiadiazole (BT) as acceptor unit and 4-hexyl-thienylenevinylene as pi conjugated bridge, S(TPA-TBTT) and S(TPA-TBTT-TPA), have been designed and synthesized for the application as donor materials in bulk-heterojunction organic solar cells (OSCs). The two molecules possess broader absorption from 350 to 700 nm benefitted from the longer pi-bridge in the molecules but weaker absorbance and poorer solubility in comparison with their corresponding organic molecules with shorter vinylene pi-bridge. The OSC based on S(TPA-TBTT): $PC_{70}BM$ (1:3, w/w) exhibited J_{sc} of 6.41 mA/cm^2, V_{oc} of 0.75 V, FF of 39.0% and power conversion efficiency of 1.90%, under the illumination of AM 1.5, 100 mW/cm^2.

1. Introduction

Bulk heterojunction organic solar cells (OSCs) based on solution-processable molecular donor materials have drawn much attention in recent years, owing to the combined advantages of the polymer solar cells (PSCs) with low cost solution-processing and the small molecule solar cells benefitted from the high purity and definite molecular weight of the organic molecules [1–24]. Among the soluble organic photovoltaic molecular materials, the star-shaped three-dimensional (3D) conjugated molecules have drawn intensive interests due to their stronger absorption and better charge-transport properties [15]. Many 3D molecules have been synthesized by attaching several conjugated chains onto a central node for the OSCs application, for examples, tetrahedral conjugated molecules based on the fixation of four conjugated thiophene chains onto a silicon node; [4] a hybrid conjugated systems consisting of a TPA core or a bithiophene node carrying thiophene chains [2]; a series of star-shaped molecules based on TPA derivative with thienylenevinylene conjugated branches and electron-withdrawing indanedione, dicyanovinyl (DCN), benzothiadiazole (BT), 2-{2,6-bis-[2-(4-styryl)-vinyl]-pyran-4-ylidene}malononitrile (DCM) or perylene imide groups [1,5,15–20,23,24]. The power conversion efficiencies (PCE) of the OSCs based on these donor materials have been reached in the range of 1.33–4.3%.

TPA-containing organic molecules have been widely investigated, in particular by Shirota, for the application as hole-transporting or electroluminescent materials [25]. Owing to its good solubility benefitted from its propeller structure, and high hole mobility, TPA is a good choice as the central core for a 3D conjugated system. As we all known, benzothiadiazole (BT) is a typical electron-acceptor unit, which can link with an electron-rich unit to form low-bandgap D–A structured functional organic semiconductor materials [26]. Our group have designed and synthesized a series of D–π–A structured molecules containing TPA as the donor unit and BT as the acceptor unit for the application as solution-processable organic photovoltaic donor materials. For expanding the family of the TPA-containing star-shaped molecules, here we designed and synthesized two new TPA- and BT-containing star-shaped D–π–A molecules, S(TPA-TBTT) and S(TPA-TBTT-TPA) as shown in Scheme 1, with a longer conjugated bridge, 4-hexyl-

* Corresponding authors. Fax: +86 10 62559373.
E-mail addresses: hechang@iccas.ac.cn (C. He), liyf@iccas.ac.cn (Y. Li).

1566-1199/$ - see front matter © 2011 Elsevier B.V. All rights reserved.
doi:10.1016/j.orgel.2011.10.017

thienylvinylene, between the TPA donor and the BT acceptor units. The aim of adding 4-hexyl-thienylvinylene pi-bridge is to extend the conjugation length of the branches of the molecules for broader absorption. The two molecules do show broad absorption from 350 to 700 nm. The OSC based on S(TPA-TBTT): $PC_{70}BM$ (1:3, w/w) exhibited power conversion efficiency of 1.90%, under the illumination of AM 1.5, 100 mW/cm^2.

2. Experimental

2.1. Chemicals

N-bromosuccinimide (NBS), *n*-butyllithium (2.5 mol/L in hexane), tetra-*n*-butylammonium bromide, sodium acetate, palladium acetate and *N*,*N*-dimethyl formamide (DMF) were obtained from Acros Organics. Tetrahydrofuran (THF) was dried over Na/benzophenoneketyl and freshly distilled prior to use. Compound (**1**) was synthesized as reported in the literature [27]. Other chemicals were common commercial level and were used as received.

2.2. Synthesis

Scheme 2 shows the synthetic routes of the monomers and the two star-shaped molecules. The detailed synthetic processes are described in the following.

2.2.1. 4-(5-bromo-4-hexylthiophen-2-yl)-7-(4-hexylthiophen-2-yl)-2,1,3-benzothiadiazole (**2**)

To a solution of 4,7-di(4-hexyl-2-thienyl)-2,1,3-benzothiadiazole (3 g, 6.4 mmol) in 100 mL anhydrous chloroform was added NBS (1.14 g, 6.4 mmol) in one portion at room temperature and stirred for 12 h. The reaction

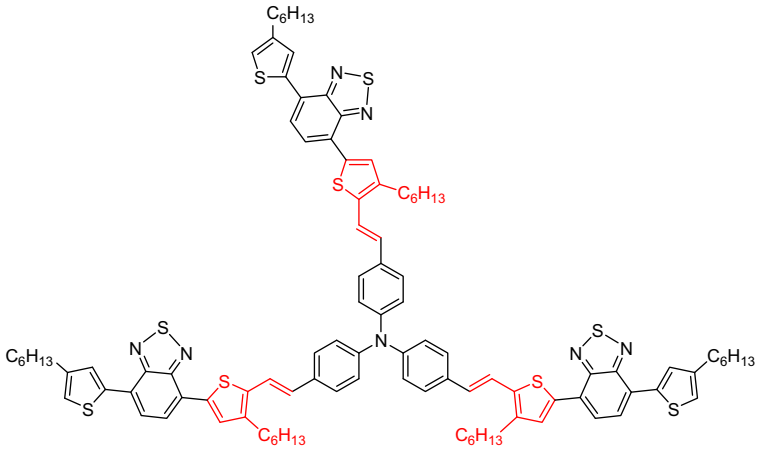

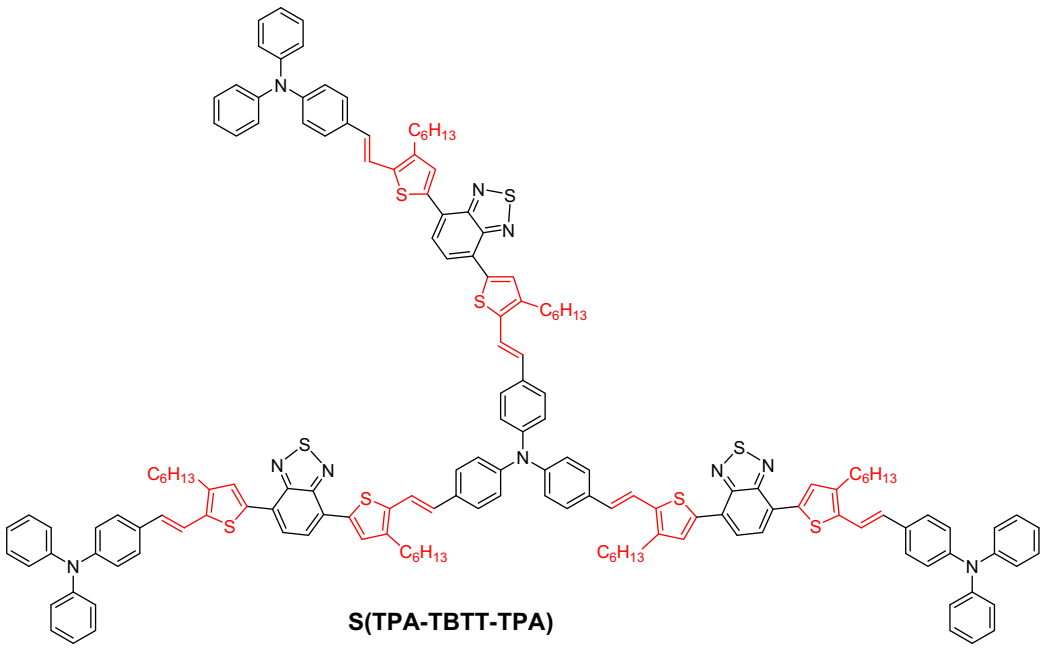

Scheme 1. Chemical structure of S(TPA-TBTT) and S(TPA-TBTT-TPA).

mixture was washed with brine and dried over anhydrous magnesium sulfate. The crude product was purified by column chromatography (petroleum ether (bp: 60–90 °C)) to give compound **2** (2 g) as dark red powder. Yield: 57%. ^{1}H NMR ($CDCl_3$, 400 MHz, δ/ppm): 7.98 (s, 1H), 7.83 (d, 1H), 7.76 (t, 2H), 7.05 (s, 1H), 2.71–2.62 (m, 4H), 1.73–1.63 (m, 4H), 1.45–1.33 (m, 12H), 0.95 (t, 6H). MALDI-TOF MS: 548.2, Calc. for $C_{26}H_{31}N_2S_3Br$ 547.6. ^{13}C NMR ($CDCl_3$, 100 MHz, δ/ppm): 152.60, 152.43, 144.53, 143.10, 138.98, 138.79, 129.30, 127.99, 126.43, 125.44, 125.04, 121.84, 111.47, 31.84, 31.78, 30.78, 30.60, 29.88, 29.83, 29.19, 29.11, 22.76, 14.24. *Anal.* Calc. for $C_{26}H_{31}N_2S_3Br$: C, 56.97; H, 5.66; N, 5.11. Found: C, 57.05; H, 5.68; N, 5.04%.

*2.2.2. 4,7-di(5-bromo-4-hexylthiophen-2-yl)-2,1,3-benzothiadiazole (**3**)*

To a solution of 4,7-di(4-hexyl-2-thienyl)-2,1,3-benzothiadiazole (3 g, 6.4 mmol) in 100 mL anhydrous chloroform was added NBS (2.39 g, 13.5 mmol) in one portion at room temperature and stirred for 12 h. The reaction mixture was washed with brine and dried by anhydrous magnesium sulfate. The crude product was purified by column chromatography (petroleum ether (bp: 60–90 °C)) to give compound **3** (2.5 g) as dark red powder. Yield: 62%. ^{1}H NMR ($CDCl_3$, 400 MHz, δ/ppm): 7.76 (d, 4H), 2.65 (t, 4H), 1.66 (m, 4H), 1.42–1.32 (m, 12H), 0.90 (t, 6H). MALDI-TOF MS: 626.1, Calc. for $C_{26}H_{30}N_2S_3Br_2$ 626.5.

*2.2.3. 4-(5-bromo-4-hexylthiophen-2-yl)-7-{5-[2-(4-diphenyl amino-phenyl)-vinyl]-4-hexylthionphene-2-yl}-2,1,3-benzothiadiazole (**4**)*

4,7-di(5-bromo-4-hexylthiophen-2-yl)-2,1,3-benzothia diazole (1 g, 1.6 mmol), *N*,*N*-diphenyl-*N*-(4-vinylphenyl) amine (432 mg, 1.6 mmol), palladium (II) acetate (10 mg), tetra-*n*-butylammonium bromide (82 mg, 0.25 mmol), and sodium acetate anhydrous (1.31 g, 16 mmol) were dissolved and kept in degassed DMF (30 ml), under argon at 80 °C for 12 h. The mixture was poured into water (30 ml). The precipitate was filtered, washed with water and dissolved in dichloromethane, dried over anhydrous sodium sulfate. After evaporation of the solvent, the residue was purified by column chromatography (petroleum/dichloromethane, 1:1) to get 812 mg compound **4**. Yield: 62.1%. ^{1}H NMR ($CDCl_3$, 400 MHz, δ/ppm): 7.94 (s, 1H), 7.81 (d, 1H), 7.76 (d, 2H), 7.39 (d, 4H), 7.27 (t, 6H), 7.13 (d, 4H), 7.04 (t, 4H), 6.99 (d, 2H), 2.74 (t, 2H), 2.64 (t, 2H), 1.72–1.63 (m, 4H), 1.42–1.34 (m, 12H), 0.90 (d, 6H). MALDI-TOF MS: 817.6, Calc. for $C_{46}H_{46}N_3S_3Br$ 816.9. ^{13}C NMR ($CDCl_3$, 100 MHz, δ/ppm): 152.60, 152.53, 147.64, 147.56, 143.15, 142.11, 138.89, 138.84, 135.90, 131.53, 130.87, 129.46, 128.35, 127.96, 127.39, 126.11, 125.15, 125.11, 124.89, 124.74, 123.62, 123.30, 118.43, 111.53, 31.88, 31.81, 31.14, 29.91, 29.87, 29.33, 29.14, 28.77, 22.81, 22.79, 14.28. *Anal.* Calc. for $C_{46}H_{46}N_3S_3Br$: C, 67.57; H, 5.63; N, 5.14. Found: C, 67.46; H, 5.71; N, 5.13%.

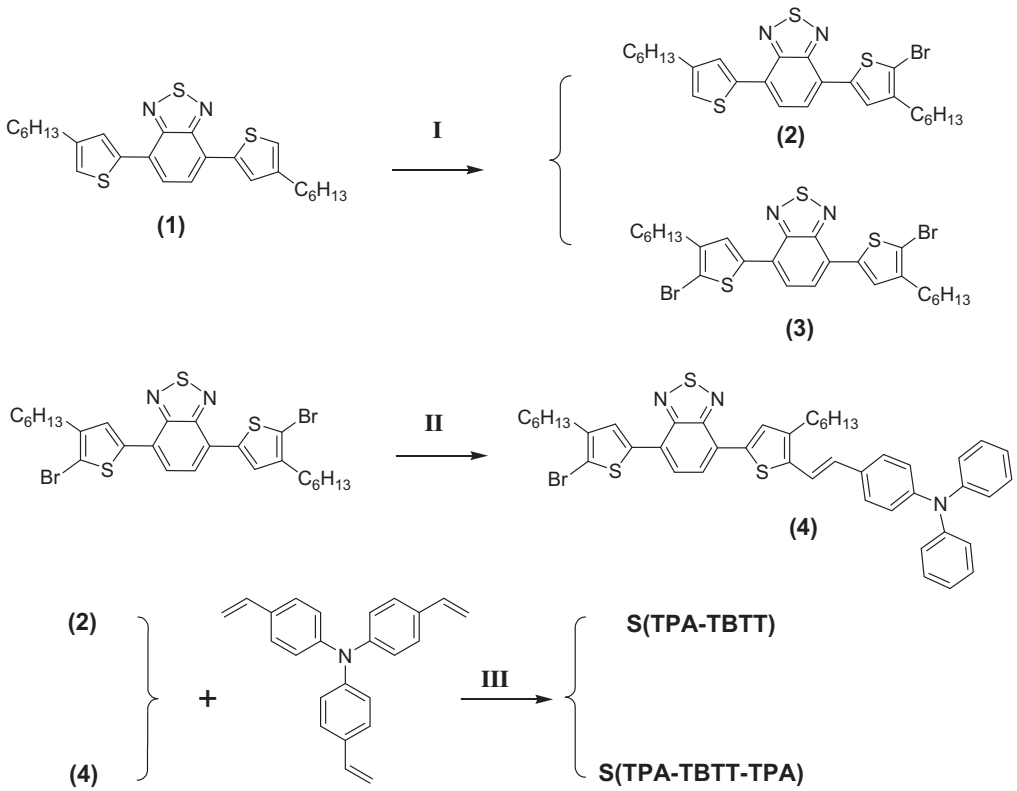

Scheme 2. Synthetic route of S(TPA-TBTT) and S(TPA-TBTT-TPA): I NBS, chloroform, room temperature for 12 h; II, III $Pd(OAc)_2$, NaOAc, *n*-Bu_4NBr, DMF, N_2, 100 °C for 24 h.

2.2.4. S(TPA-TBTT)

Compound **2** (1 g, 1.8 mmol), tris-(4-vinylphenyl)amine (161 mg, 0.5 mmol), palladium (II) acetate (10 mg), tetra-*n*-butylammonium bromide (77 mg, 0.24 mmol), and sodium acetate anhydrous (1.23 g, 15 mmol) were dissolved and kept in degassed DMF (30 ml), under argon at 100 °C for 24 h. The mixture was poured into water (30 ml). The precipitate was filtered, washed with water and dissolved in dichloromethane, dried over anhydrous sodium sulfate. After evaporation of the solvent, the residue was purified by column chromatography (petroleum/dichloromethane, 1:1) to get 205 mg S(TPA-TBTT). Yield: 23.8%. ^{1}H NMR ($CDCl_3$, 400 MHz, δ/ppm): 7.98–7.95 (d, 6H), 7.85–7.82 (d, 6H), 7.44–7.42 (d, 6H), 7.20–7.09 (m, 9H), 7.04–6.98 (t, 6H), 2.76–2.67 (m, 12H), 1.72–1.69 (t, 12H), 1.42–1.34 (m, 36H), 0.90–0.86 (t, 18H). MALDI-TOF MS: 1722.0, Calc. for $C_{102}H_{111}N_7S_9$ 1722.6. ^{13}C NMR ($CDCl_3$, 100 MHz, δ/ppm): 152.76, 146.72, 144.56, 142.31, 139.23, 138.50, 136.29, 132.49, 130.70, 129.17, 128.03, 127.53, 126.06, 125.79, 125.69, 125.41, 124.51, 121.74, 118.95, 31.90, 31.89, 31.19, 30.84, 30.65, 29.87, 29.35, 29.23, 28.82, 22.81, 14.30. *Anal.* Calc. for $C_{102}H_{111}N_7S_9$: C, 69.07; H, 6.45; N, 5.53. Found: C, 70.00; H, 6.97; N, 4.99%.

2.2.5. S(TPA-TBTT-TPA)

Compound **4** (1 g, 1.2 mmol), tris-(4-vinylphenyl)amine (119 mg, 0.37 mmol), palladium (II) acetate (15 mg), tetra-*n*-butylammonium bromide (58 mg, 0.18 mmol), and sodium acetate anhydrous (910 mg, 11 mmol) were dissolved and kept in degassed DMF (30 ml), under argon at 100 °C for 24 h. The mixture was poured into water (30 ml). The precipitate was filtered, washed with water and dissolved in dichloromethane, dried over anhydrous sodium sulfate. After evaporation of the solvent, the residue was purified by column chromatography (petroleum/dichloromethane, 1:1) to get 96 mg S(TPA-TBTT-TPA). Yield: 10.3%. ^{1}H NMR ($CDCl_3$, 400 MHz, δ/ppm): 7.95–7.81 (d, 12H), 7.44–7.26 (m, 30H), 7.20–7.15 (d, 6H), 7.13–7.11 (12H), 7.06–6.95 (m, 24H), 2.74 (t, 12H), 1.69 (t, 12H), 1.42–1.34 (m, 36H), 0.90 (t, 18H). MALDI-TOF MS: 2530.2, Calc. for $C_{162}H_{156}N_{10}S_9$ 2530. ^{13}C NMR ($CDCl_3$, 100 MHz, δ/ppm): 152.65, 147.50, 145.91, 145.10, 143.41, 133.40, 131.90, 131.44, 130.54, 129.75, 129.31, 127.22, 126.63, 125.22, 124.58, 123.50, 123.13, 31.73, 31.00, 29.71, 29.18, 28.64, 22.65, 14.13. *Anal.* Calc. for $C_{162}H_{156}N_{10}S_9$: C, 76.83; H, 6.17; N, 5.53. Found: C, 76.05; H, 6.10; N, 5.25%.

2.3. Measurements

Nuclear magnetic resonance (NMR) spectra were taken on a Bruker DMX-400 spectrometer. MALDI-TOF spectra were recorded on a Bruker BIFLEXIII. Elemental analyses were carried out on a flash EA 1112 elemental analyzer. Absorption spectra were taken on a Hitachi U-3010 UV–Vis spectrophotometer. The film on quartz used for UV measurements was prepared by spin-coating with chloroform solution. The TGA measurement was performed on a Perkin–Elmer TGA-7 apparatus. The electrochemical cyclic voltammogram was obtained using a Zahner IM6e electrochemical workstation in a 0.1 mol/L tetrabutylammonium hexafluorophosphate (Bu_4NPF_6) acetonitrile solution. A Pt electrode coated with the sample film was used as the working electrode, a Pt wire and Ag/Ag^+ (0.01 M $AgNO_3$ in acetonitrile) were used as the counter and reference electrodes respectively.

2.4. Fabrication and characterization of organic solar cells

Organic solar cells (OSCs) were fabricated in the configuration of the traditional sandwich structure with an ITO positive electrode and a metal negative electrode. Patterned ITO glass with a sheet resistance of ca. 10 Ω sq^{-1} was purchased from CSG Holding Co., Ltd. (China). The ITO glass was cleaned in an ultrasonic bath of acetone and isopropanol, and treated by UVO (ultraviolet ozone cleaner, Jelight Company, USA). Then a thin layer (30 nm) of PEDOT: PSS (poly(3,4-ethylenedioxythiophene)-poly(styrene sulfonate)) (Baytron PVP AI 4083, Germany) was spin-coated on the ITO glass. Subsequently, the photosensitive layer was prepared by spin-coating the blend chlorobenzene solution of S(TPA-TBTT): $PC_{70}BM$ (1:3 w/w) or S(TPA-TBTT-TPA): $PC_{70}BM$ (1:3 w/w) on the top of the PEDOT:PSS layer and baked at 80 °C for 0.5 h. The thickness of the photoactive layer was measured using an Ambios Technology XP-2 profilometer. Finally, a metal electrode layer of Al (ca. 120 nm) was vacuum evaporated on the photoactive layer under a shadow mask in the vacuum of ca. 10^{-4} Pa. The current–voltage (I–V) measurement of the devices was conducted on a computer-controlled Keithley 236 Source Measure Unit. A xenon lamp coupled with A.M. 1.5 solar spectrum filters was used as light source, and the optical power at the sample was 100 mW/cm^2.

3. Results and discussion

3.1. Synthesis and thermal stability of the molecules

S(TPA-TBTT) and S(TPA-TBTT-TPA) were synthesized according to the synthetic routes as shown in Scheme 2. The yields of S(TPA-TBTT) and S(TPA-TBTT-TPA) are 23.8% and 10.3%, respectively. The low yields could be due to the side-products of one armed and two armed molecules. The two materials are soluble in common organic solvents, such as $CHCl_3$, THF, chlorobenzene and toluene. But S(TPA-TBTT-TPA) exhibits poorer solubility than S(TPA-TBTT). The thermal stability of the compounds was investigated by thermogravimetric analysis (TGA). The temperatures with 5% weight loss are at 345 and 308 °C for S(TPA-TBTT) and S(TPA-TBTT-TPA), respectively, as shown in Fig. 1. The stability of the materials is good enough for the application in optoelectronic devices. S(TPA-TBTT-TPA) shows lower 5%-weight-loss-temperature than S(TPA-TBTT). The reason may be more content of ethylene unit in S(TPA-TBTT-TPA).

3.2. Absorption spectra

Fig. 2 shows the UV–Vis absorption spectra of S(TPA-TBTT) and S(TPA-TBTT-TPA) in chloroform solution and film state. The optical absorption maxima (λ) were summarized in Table 1. Benefited from their D–A molecular structure connected with longer conjugated bridge, the molecules

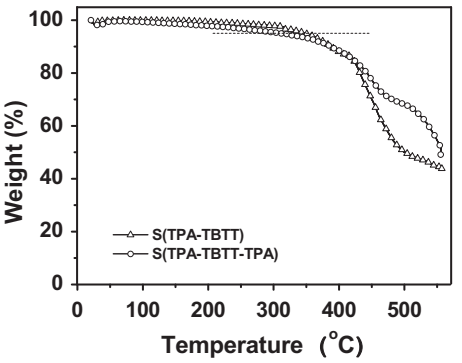

Fig. 1. TGA plots of S(TPA-TBTT) and S(TPA-TBTT-TPA).

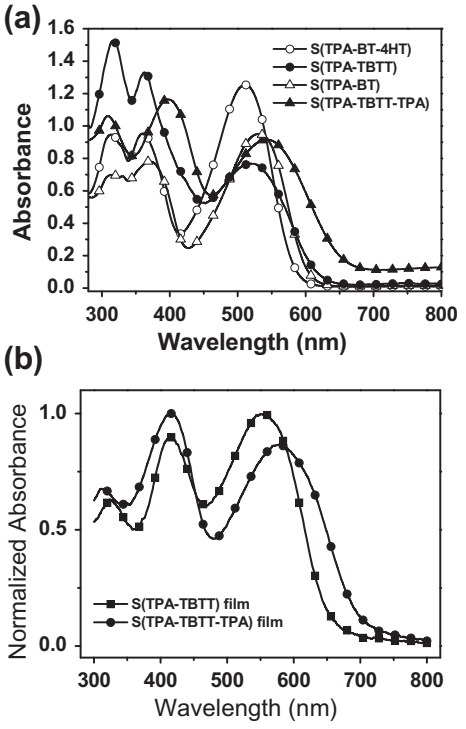

Fig. 2. (a) absorption spectra of S(TPA-BT-4HT), S(TPA-TBTT), S(TPA-BT) and S(TPA-TBTT-TPA) in chloroform solution at a concentration of 10^{-5} mol/L; (b) normalized absorption spectra of S(TPA-TBTT) and S(TPA-TBTT-TPA) films.

in chloroform solution exhibit strong absorption in the wavelength range from 350 to 650 nm. The absorption in the wavelength range of 300–450 nm corresponds to the π–π^* absorption of the molecules, and the visible absorption peak between 450 and 650 nm could be assigned to the intramolecular charge-transfer (ICT) absorption between the TPA moiety and BT moiety. Compared with the absorption peak at 509 nm of S(TPA-BT-4HT) [18] and 531 nm of S(TPA-BT) [15] where the pi-bridge is vinylene unit, the absorption peak of S(TPA-TBTT) (544 nm) and S(TPA-TBTT-TPA) (560) is red-shifted by ca. 30–40 nm, which implies that the longer thienylenevinylene pi-bridge

Table 1
Solution (CHCl3) and thin-film (glass substrate) optical absorption maxima (λ), optical energy gap (E_g^{opt}), onset oxidation potential (E_{onset}^{ox}), HOMO and LUMO energy levels of S(TPA-TBTT) and S(TPA-TBTT-TPA).

Compounds	$\lambda_{solution}$ (nm)	λ_{film} (nm)	$(E_g^{opt})_{film}$ (eV)	E^{ox}_{onset} (V *vs* Ag/Ag$^+$) /HOMO (eV)	LUMO[a] (eV)
S(TPA-TBTT)	402, 544	414, 552	1.88	0.59/−5.30	−3.42
S(TPA-TBTT-TPA)	410, 560	416, 576	1.76	0.43/−5.14	−3.38

[a] LUMO energy level was calculated from the HOMO level and optical energy gap: LUMO = HOMO + E_g^{opt}

in S(TPA-TBTT) and S(TPA-TBTT-TPA) broadened the absorption. However, the absorptivity of the two compounds decreased in comparison with the corresponding molecules with vinylene pi-bridge. The molar absorptivity of S(TPA-TBTT) and S(TPA-TBTT-TPA) is 7.69×10^4 and 9.16×10^4 respectively, in comparison with 12.4×10^4 for S(TPA-BT-4HT) and 9.51×10^4 for S(TPA-BT). Probably, the longer pi-bridge between the TPA donor and BT acceptor units in S(TPA-TBTT) and S(TPA-TBTT-TPA) reduced the ICT absorption band, which results in the lower absorptivity of the two compounds. The absorption spectra of the two molecule films are red-shifted a little than their solutions, which indicate some aggregation of the molecules in the film state existed. Consistent with the absorption spectra of the solutions, the absorption maxima of S(TPA-TBTT) (552 nm) film is also red-shifted by 23 nm than that (529 nm) of S(TPA-BT-4HT) film [18] and that (576 nm) of S(TPA-TBTT-TPA) film is red-shifted by 35 nm than that (541 nm) of S(TPA-BT) film [15]. The absorption edge of S(TPA-TBTT) and S(TPA-TBTT-TPA) films are at ca. 659 and 706 nm, corresponding to the band gap of 1.88 and 1.76 eV, respectively.

3.3. Electrochemical properties

Electrochemical cyclic voltammetry was carried out for S(TPA-TBTT) and S(TPA-TBTT-TPA) films on Pt electrode, in order to measure the HOMO energy levels of them. Fig. 3 shows the cyclic voltammograms of S(TPA-TBTT) and S(TPA-TBTT-TPA) films. The values of the onset oxidation potential (E^{ox}_{onset}) and the HOMO of the compounds are listed in Table 1. The HOMO and LUMO energy levels of S(TPA-TBTT) were estimated to be −5.30 and −3.42 eV, respectively, from the onset oxidation and optical energy gap according to the following equations: $E_{HOMO} = -e(E^{ox}_{onset} + 4.71)$(eV) [28], E_{LUMO} = HOMO + E_g^{opt}(eV). The HOMO and LUMO energy levels were −5.14 and −3.38 eV for S(TPA-TBTT-TPA). Compared with the HOMO and LUMO energy levels for $PC_{70}BM$, the two compounds are suitable to be used as the photovoltaic donors.

3.4. AFM morphology

Morphology of the photoactive layer is very important for the photovoltaic performance of OSCs [29,30]. We used atomic force microscopy (AFM) to investigate the

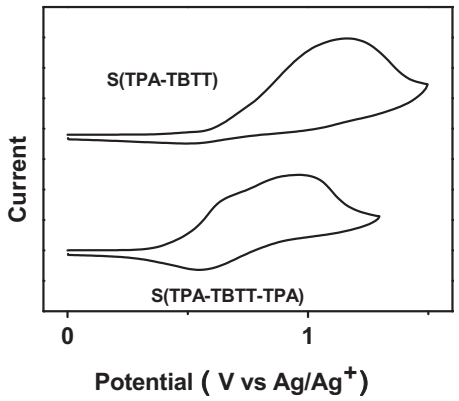

Fig. 3. Cyclic voltammogram of S(TPA-TBTT) and S(TPA-TBTT-TPA) film on Pt electrode in an acetonitrile solution of 0.1 mol/L *n*-Bu_4NPF_6 (*n*-Bu=butyl) with a scan rate of 100 mV/s.

morphology of the star-shaped molecules: $PC_{70}BM$ (1:3, w/w) blend films, as shown in Fig. 4. The AFM images of the blend films exhibit typical amorphous morphology without any crystalline domains. The surface roughness (RMS) of the blend film of S(TPA-TBTT)/$PC_{70}BM$ was 5.28 nm, while RMS of the film of S(TPA-TBTT-TPA)/$PC_{70}BM$ was 16.4 nm. The rougher morphology of S(TPA-TBTT-TPA) could result from its poorer solubility.

3.5. Photovoltaic properties

Bulk-heterojunction OSCs were fabricated by using S(TPA-TBTT) or S(TPA-TBTT-TPA) as donor materials, $PC_{70}BM$ as acceptor material and Al as the negative electrode, respectively. The device structure is ITO/PEDOT: PSS/photoactive layer (60 nm)/Al. Fig. 5 show the typical current–voltage curves of the OSCs under the illumination of AM 1.5, 100 mW/cm^2. The photovoltaic performance data of the OSCs, including V_{oc}, J_{sc}, FF and PCE values, are summarized in Table 2. The best photovoltaic performance of the OSCs based on blends of S(TPA-TBTT): $PC_{70}BM$ (1:3, w/w) exhibited J_{sc} of 6.41 mA/cm^2, V_{oc} = 0.75, FF = 39.0%, PCE = 1.90%, under the illumination of AM 1.5, 100 mW/cm^2. The OSC based on S(TPA-TBTT-TPA): $PC_{70}BM$ (1:3, w/w) shows a J_{sc} = 5.41 mA/cm^2, a V_{oc} = 0.71, FF = 32.0%, PCE = 1.23%. S(TPA-TBTT-TPA) showed lower J_{sc} and poorer photovoltaic performance, due probably to its poorer solubility and rough morphology mentioned above. In addition, hole mobility of S(TPA-TBTT-TPA) could be low because of its poorer solubility, which should also result in the lower J_{sc}. In comparison with the vinylene pi-bridged molecules S(TPA-BT-4HT) and S(TPA-BT), the longer thienylenevinylene pi-bridged molecules S(TPA-TBTT) and S(TPA-TBTT-TPA) did not exhibit better photovoltaic performance, although they possess broader absorption. The reason may be as fellows: firstly, the absorbance of S(TPA-TBTT) and S(TPA-TBTT-TPA) dropped significantly than that of S(TPA-BT-4HT) and S(TPA-BT), which will result in lower J_{sc} of the OSCs; secondly, along with the increase of the size (longer pi-bridge) for S(TPA-TBTT) and S(TPA-TBTT-TPA), their solubility decreased which will influence the

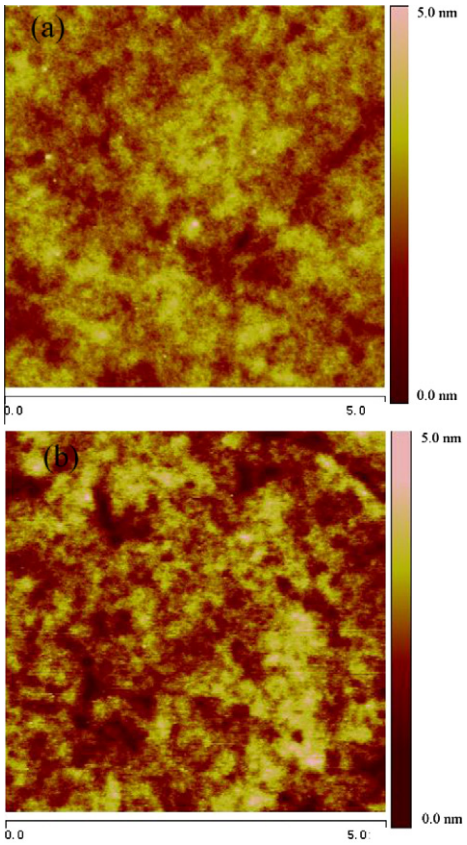

Fig. 4. AFM images of star molecules: $PC_{70}BM$ films spin-coated from the blend solution: (a) S(TPA-TBTT)/$PC_{70}BM$. (b) S(TPA-TBTT-TPA)/$PC_{70}BM$. Both of the films were spin-coated on ITO/PEDOT: PSS substrates and the scan size for the images is 5 × 5 μm.

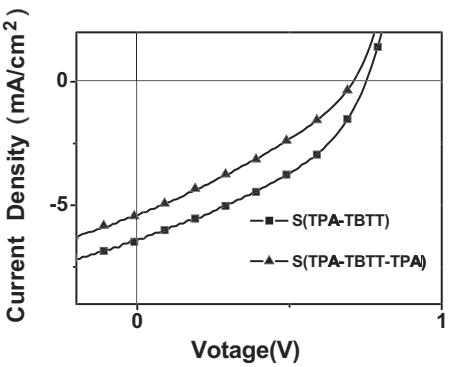

Fig. 5. Current density–voltage characteristics of the OSCs based on the blend of S(TPA-TBTT) or S(TPA-TBTT-TPA)/$PC_{70}BM$ (1:3, w/w) with Al as the negative electrode under the illumination of AM 1.5, 100 mW/cm^2.

film-forming properties of the materials. As we all know, the morphology of the photoactive layer is very important for the photovoltaic performance of OSCs. The result indicated that broad absorption, strong absorbance and good solubility all are important for the solution-processable

Table 2
Photovoltaic performance of ITO/PEDOT: PSS/S(TPA-TBTT) or S(TPA-TBTT-TPA): $PC_{70}BM$ (1:3, w/w)/Al under the illumination of AM 1.5, 100 mW/cm^2.

Active layer	V_{oc} (V)	J_{sc} (mA/cm^2)	FF (%)	PCE (%)
S(TPA-TBTT): $PC_{70}BM$ (1:3, w/w)	0.75	6.41	39.0	1.90
S(TPA-TBTT-TPA): $PC_{70}BM$ (1:3, w/w)	0.71	5.41	32.0	1.23

organic molecules used in OSCs. In considering the effect of the molecular structure on the photovoltaic performance of the star-shaped molecules with D–π–A structure, the length of the pi-bridge between the donor and acceptor units are very important. Too big pi-bridge, such as the thienylenevinylene pi-bridge in S(TPA-TBTT) and S(TPA-TBTT-TPA), will weaken the ICT absorption band and lead to larger molecular size, poorer solubility and rougher morphology, which results in poorer photovoltaic performance of the molecules.

4. Conclusions

Two solution-processable star-shaped D–π–A molecules with triphenylamine (TPA) as donor unit, benzothiadiazole (BT) as acceptor unit and 4-hexyl-thiophenevinylene as conjugated π bridge, S(TPA-TBTT) and S(TPA-TBTT-TPA), have been designed and synthesized for the application in solution-processable organic solar cells (OSCs). The two organic materials possess high stability, broad absorption from 350 to 700 nm and suitable energy levels for the application as donor materials in OSCs. The OSC devices based on the blend of S(TPA-TBTT): $PC_{70}BM$ (1:3, w/w) or S(TPA-TBTT-TPA): $PC_{70}BM$ (1:3, w/w) exhibited J_{sc} of 6.41 and 5.41 mA/cm^2, V_{oc} of 0.75 and 0.71 V, FF of 39.0% and 32.0%, PCE of 1.90% and 1.23%, respectively, under the illumination of AM 1.5, 100 mW/cm^2. The results indicate that broad absorption, strong absorbance and good solubility all are important for the solution-processable organic molecules used in OSCs.

Acknowledgments

This work was supported by NSFC (Nos. 50803071, 20874106, 50933003 and 21021091), Ministry of Science and Technology of China, and the Chinese Academy of Sciences.

References

[1] S. Roquet, A. Cravino, P. Leriche, O. Aleveque, P. Frere, J. Roncali, J. Am. Chem. Soc. 128 (2006) 3459–3466.
[2] A. Cravino, S. Roquet, O. Aleveque, P. Leriche, P. Frere, J. Roncali, Chem. Mater. 18 (2006) 2584–2590.
[3] S. Karpe, A. Cravino, P. Frere, M. Allain, G. Mabon, J. Roncali, Adv. Funct. Mater. 17 (2007) 1163–1171.
[4] J. Roncali, P. Leriche, A. Cravino, Adv. Mater. 19 (2007) 2045–2060.
[5] A. Petrella, J. Cremer, L.D. Cola, P. Bauerle, R.M. Williams, J. Phys. Chem. A 109 (2005) 11687–11695.
[6] C.-Q. Ma, E. Mena-Osteritz, T. Debaerdemaeker, M.M. Wienk, R.N.J. Janssen, P. Bauerle, Angew. Chem. Int. Ed. 46 (2007) 1679–1683.
[7] C.-Q. Ma, M. Fonrodona, M.C. Schikora, M.M. Wienk, R.A.J. Janssen, P. Bauerle, Adv. Funct. Mater. 18 (2008) 3323–3331.
[8] M.L. Sun, L. Wang, X.H. Zhu, B. Du, R. Liu, W. Yang, Y. Cao, Sol. Energy Mater. Sol. Cells 91 (2007) 1681–1687.
[9] X. Sun, Y. Zhou, W. Wu, Y. Liu, W. Tian, G. Yu, W. Qiu, S. Chen, D. Zhu, J. Phys. Chem. B 110 (2006) 7702–7707.
[10] L.L. Xue, J.T. He, X. Gu, Z.F. Yang, B. Xu, W.J. Tian, J. Phys. Chem. C 113 (2009) 12911–12917.
[11] A.B. Tamayo, B. Walker, T.Q. Nguyen, J. Phys. Chem. C 112 (2008) 11545–11551.
[12] A.B. Tamayo, X.D. Dang, B. Walker, J. Seo, T. Kent, T.Q. Nguyen, Appl. Phys. Lett. 94 (2009) (Art. No. 103301).
[13] B. Walker, A.B. Tomayo, X.D. Dang, P. Zalar, J.H. Seo, A. Garcia, M. Tantiwiwat, T.Q. Nguyen, Adv. Funct. Mater. 19 (2009) 3063–3069.
[14] C. He, Q.G. He, X.D. Yang, G.L. Wu, C.H. Yang, F.L. Bai, Z.G. Shuai, L.X. Wang, Y.F. Li, J. Phys. Chem. C 111 (2007) 8661–8666.
[15] C. He, Q.G. He, Y.P. Yi, G.L. Wu, F.L. Bai, Z.G. Shuai, Y.F. Li, J. Mater. Chem. 18 (2008) 4085–4090.
[16] G.J. Zhao, G.L. Wu, C. He, F.Q. Bai, H.X. Xi, H.X. Zhang, Y.F. Li, J. Phys. Chem. C 113 (2009) 2636–2642.
[17] G.L. Wu, G.J. Zhao, C. He, J. Zhang, Q.G. He, X.M. Chen, Y.F. Li, Sol. Energy Mater. Sol. Cells 93 (2009) 108–113.
[18] J. Zhang, Y. Yang, C. He, Y.J. He, G.J. Zhao, Y.F. Li, Macromolecules 42 (2009) 7619–7622.
[19] Y. Yang, J. Zhang, Y. Zhou, G.J. Zhao, C. He, Y.F. Li, M. Andersson, O. Inganas, F.L. Zhang, J. Phys. Chem. C 114 (2010) 3701–3706.
[20] J. Zhang, D. Den, C. He, M.J. Zhang, Z.G. Zhang, Z.J. Zhang, Y.F. Li, Chem. Mater. 23 (2011) 817–822.
[21] J. Zhang, G.L. Wu, C. He, D. Deng, Y.F. Li, J. Mater. Chem. 21 (2011) 3768–3774.
[22] H.X. Shang, H.J. Fan, Q.Q. Shi, S. Li, Y.F. Li, X.W. Zhan, Sol. Energy Mater. Sol. Cells 94 (2010) 457–464.
[23] H.X. Shang, H.J. Fan, Y. Liu, W.P. Hu, Y.F. Li, X.W. Zhan, Adv. Mater. 23 (2011) 1554–1557.
[24] E. Ripaud, T. Rousseau, P. Leriche, J. Roncali, Adv. Energy Mater. 1 (2011) 540–545.
[25] Y. Shirota, J. Mater. Chem. 15 (2005) 75–93.
[26] M. Karikomi, C. Kitamura, S. Tanaka, Y. Yamashita, J. Am. Chem. Soc. 117 (1995) 6791–6792.
[27] Q. Hou, Q.M. Zhou, Y. Zhang, W. Yang, R.Q. Yang, Y. Cao, Macromolecules 37 (2004) 6299–6305.
[28] Q.J. Sun, H.Q. Wang, C.H. Yang, Y.F. Li, J. Mater. Chem. 13 (2003) 800–806.
[29] W.L. Ma, C.Y. Yang, X. Gong, K. Lee, A.J. Heeger, Adv. Funct. Mater. 15 (2005) 1617–1622.
[30] G. Li, V. Shrotriya, J.S. Huang, Y. Yao, T. Moriarty, K. Emery, Y. Yang, Nat. Mater. 4 (2005) 864–868.